Enhancement of Photogenerated Electron Transport in Dye-Sensitized Solar Cells with Introduction of a Reduced Graphene Oxide-TiO2 Junction

ARTICLE *in* CHEMISTRY - A EUROPEAN JOURNAL · JANUARY 2011

Impact Factor: 5.73

ACS APPLIED MATERIALS & INTERFACES

Research Article

www.acsami.org

Improved Utilization of Photogenerated Charge Using Fluorine-Doped TiO_2 Hollow Spheres Scattering Layer in Dye-Sensitized Solar Cells

Junling Song,[†,‡,#] Hong Bin Yang,[†,#] Xiu Wang,[§] Si Yun Khoo,[†] C. C. Wong,*[,§] Xue-Wei Liu,*[,‡] and Chang Ming Li*[,†,⊥,¶]

[†]School of Chemical and Biomedical Engineering, Nanyang Technological University, 70 Nanyang Drive, Singapore 637457

[‡]School of Physical & Mathematical Sciences, Nanyang Technological University, Singapore 637371

[§]School of Materials Science and Engineering, Nanyang Technological University, Singapore 639798

[⊥]Institute for Clean Energy & Advanced Materials, Southwest University, Chongqing 400715, P.R. China

[¶]Chongqing Key Laboratory for Advanced Materials and Technologies of Clean Energies, Chongqing 400715, P.R. China

ABSTRACT: We demonstrate a strategy to improve utilization of photogenerated charge in dye-sensitized solar cells (DSSCs) with fluorine-doped TiO_2 hollow spheres as the scattering layer, which improves the fill factor from 69.4% to 74.1% and in turn results in an overall efficiency of photoanode increased by 13% (from 5.62% to 6.31%) in comparison with the control device using undoped TiO_2 hollow spheres. It is proposed that the fluorine-doping improves the charge transfer and inhibition of charge recombination to enhance the utilization of the photogenerated charge in the photoanode.

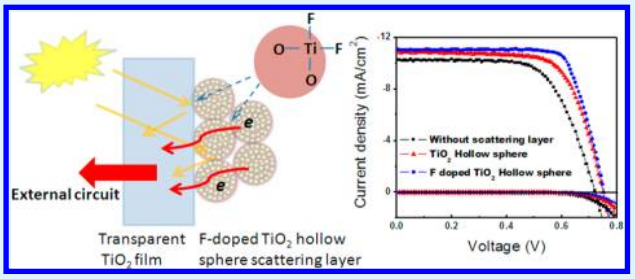

KEYWORDS: *dye-sensitized solar cells, scattering layer, electron transport, fluorine-doping, charge recombination, AC impedance*

1. INTRODUCTION

Dye-sensitized solar cells (DSSCs) have attracted much attention because of their cost advantage in comparison with first generation solar cells.[1−8] In this type of solar cell, under illumination, the dye-absorbed semiconductor transports electron to the counter electrode accompanied with the hole eliminated by the redox reaction at the electrode/electrolyte interface. Therefore, rational design of the semiconducting electrode is crucial to improve the overall power conversion efficiency of devices.[9−12] Much effort has been devoted to increase the surface area or the thickness of photoanode for better light utility and thus higher photocurrent. However, unlimited increase of the electrode thickness is augmentation of a negative effect from an increased cell series resistance caused by an increased path-length between the electrons and the redox couple in the electrolyte. Various types of scattering layers such as photonic crystals and different metal oxide spheres[13−18] have been introduced to increase the absorption path-length of photons, create confinement property for enhancement of light harvesting, avoid the increment in series resistance, and enhance recombination probability.

However, the introduced transparent/light-scattering TiO_2 heterogeneous double layer architecture usually causes additional interfacial resistance between scattering layer and nanoporous TiO_2 film, leading to low utilization of photogenerated electrons in the scattering layer. In order to obtain better device performance, it is necessary to enhance the electron transportation across the scattering layer to the nanoporous TiO_2 film, and then, the mesoporous TiO_2 can act as the light-scattering center as well as the electricity-generation source. Recently, studies have shown that an effective way to improve charge collection is by reducing the trap states[19] in semiconductor via heteroatom-doping.[20−25] According to our previous study, TiF_4 hydrolysis treatment of the photoanode could reduce the charge recombination and contact resistance.[26] Herein, we design a photoanode with fluorine-doped (F-doped) TiO_2 hollow nanoparticles coated on the top of the transparent TiO_2 nanoparticles layer to form the compact multifunctional photoanode. The electron and electrolyte transfer in this photoanode were studied by electrochemical impedance spectra (EIS). The results indicate that the F-doped hollow TiO_2 scattering layer significantly enhances the cell efficiency by decreasing the contact resistance between scattering layer and bottom transparent TiO_2 film.

2. EXPERIMENTAL SECTION

2.1. Materials. Titanium(IV) fluoride and hexadecylamine (HDA, 98%) were purchased from Sigma-Aldrich. Titanium(IV) *i*-propoxide (TTIP, 98%) was purchased from Sterm Chemicals. Absolute ethanol (AR, Fisher Scientific), potassium chloride (AR, Fisher Scientific),

Received: May 8, 2012
Accepted: June 25, 2012
Published: June 25, 2012

   dx.doi.org/10.1021/am300801f | ACS Appl. Mater. Interfaces 2012, 4, 3712−3717

ammonia solution (25 wt %, Fisher Scientific), and Milli-Q water (18.2 MΩ cm) were used for the synthesis.

2.2. Preparation of TiO_2 Hollow Spheres and F-Doped TiO_2 Hollow Spheres. Titanium(IV) *i*-propoxide (TTIP, 2.0 mmol), Titanium(IV) fluoride (0.4 mmol was added as F source for F-doped TiO_2 hollow spheres), and urea (4.0 mmol) were dissolved in 15 mL of ethanol. *tert*-Butyl ammonium hydroxide, 1.0 M solution in methanol (TBAH, 4.0 mmol, Sigma Aldrich), was added slowly into the solution. The mixture was stirred for 30 min to obtain a clear solution. Then, the mixture was processed by the hydrothermal method at 180 °C for 24 h. The white precipitate was cooled to room temperature, filtered, and washed several times with ethanol. The filtered white powdery titanium oxide was then sintered at 500 °C for 2 h in air.

2.3. Synthesis of Titanium Oxide and F-doped Titanium Oxide Hollow Sphere Gel. Ethylcellulose 200 cPa (0.5 g) and ethanol (5.0 mL) were stirred to form a clear gel. Titanium oxide or F-doped titanium oxide hollow sphere (0.1 g) and terpineol (0.4 g) were then added into the mixture and stirred continually to form a homogeneous white gel.

2.4. Preparation of Photoanode and Cell Assembly. Briefly, transparent conducting glass (SnO_2:F, FTO, 15 Ω/square, Solaronix) was cleaned in isopropyl alcohol and 0.1 M HCl solution using an ultrasonic bath for 30 min, respectively, and rinsed with water and ethanol. After treatment in a UV-ozone system (Model No. 256-220, Jelight Company) for 15 min, the FTO glass was immersed into 40 mM $TiCl_4$ solution at 70 °C for 30 min. Then, the 13.0 μm thick TiO_2 (Ti-Nanoxide T/SP, Solaronix) electrodes were prepared by the doctor blading technique and gradually annealed under static air flow at 325 °C for 5 min, 375 °C for 5 min, 450 °C for 15 min, and 500 °C for 15 min according to the method as reported.[2] A TiO_2 scattering layer was coated on top of the transparent TiO_2 film and then treated by 40 mM $TiCl_4$ solution at 70 °C for another 30 min and sintered at 500 °C for 30 min. The electrodes were cooled to 80 °C and then immersed in 0.3 mM Z907 in acetonitrile/*tert*-butyl alcohol (1:1) for 10 h. Rinsed with acetonitrile, the photoanodes were bonded together with platinized conducting glass (400 Å Pt fabricated by e-beam evaporation on the glass) using 60 μm thermal-plastic Suryln spacers. The areas of the electrodes were around 0.16 cm^2. The ionic liquid electrolyte (EL-HPE) was introduced into the sandwich cells.

2.5. Characterization of Samples. The morphologies of TiO_2 spheres and films were studied by field emission scanning electron microscopy (FESEM, JEOL JSM-6360) and transmission electron microscopy (TEM, JEOL, JEM-1400). Powder X-ray diffraction (XRD) measurements were carried out using a Rikaku Rint-2000 instrument with Cu Kα radiation. Nitrogen adsorption−desorption isotherms were obtained by ASAP 2020 (Micromeritics Instrument Corp.) apparatus. All the samples were degassed at 200 °C prior to Brunauer−Emmett−Teller (BET) measurements. The fluorine doping level of the sample was determined by X-ray photoelectron spectroscopy (XPS; KRATOS, AXIS ULTRA) using a monochromatized Al Kα (1486.7 eV) X-ray source. The current−voltage characteristics of the cell under 100 mW cm^{-2} (AM 1.5) conditions provided by Sun 2000 solar simulator (Abet-technologies, U.S.A.) were obtained by applying external potential bias to the cell, and the generated photocurrent was measured by a Keithley model 2440 digital source meter (Keithley, U.S.A.). The data was recorded using lab tracer software. The incident photon-to-current efficiency (IPCE) was obtained with Oriel QE/IPCE Kit equipment (Oriel, U.S.A.). Electrical impedance experiments were carried out in the dark and under illumination conditions with an autolab electrochemical workstation with a frequency range from 0.01 Hz to 0.1 MHz and a potential modulation of 20 mV. The forward bias is −0.69 V, and open-circuit voltage is in the dark and under illumination condition, respectively.

3. RESULTS AND DISCUSSION

The F doping effect on the HS morphology was first studied by SEM. As shown in Figure 1, the morphology of TiO_2 is not changed observably with F doping. The F-doped and undoped HS TiO_2 are composed of ca. 3 μm spheres with fragmentized parts. BET nitrogen gas adsorption technique was employed to determine the specific surface area of different TiO_2 structures. The HS and F-HS TiO_2 have nearly the same specific surface area and porosity, which are 77.1 m^2/g and 70.0% for HS and 78.3 m^2/g and 71.5% for F-HS TiO_2, respectively. These results indicate the F doping does not significantly influence the morphology and specific surface area of TiO_2 hollow sphere; thus, it will not cause dramatic change on the dye loading ability and light scattering effect of HS.

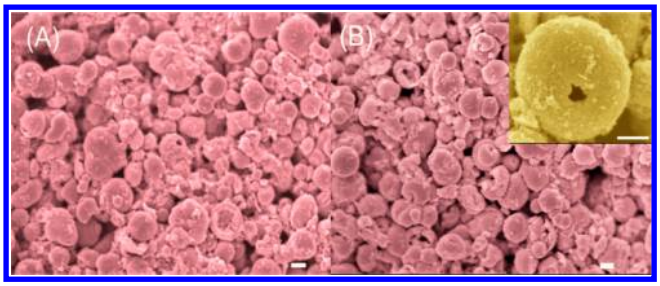

Figure 1. SEM images of undoped (a) and fluorine doped (b) TiO_2 hollow sphere (F-HS). Inset is the SEM image of single TiO_2 hollow sphere (F-HS). Scale bars in figures represent 1 μm.

The F doping state in TiO_2 HS structure was investigated by X-ray Photoelectron Spectroscopy (XPS). As shown in Figure 2a, besides the peaks at ∼460 eV corresponding to the energies of the photoelectrons of Ti^{4+}, the peaks at ∼530 and 980 eV are attributed to the O 1s and O KLL, respectively.[19,27,28] A small peak at ∼685 eV is observed in F-HS TiO_2 attributing to F1s. Figure 2b shows the high-resolution XPS spectra of F 1s region, beside a F 1s peak at 684.6 eV; no additional peaks are identified at higher energies. Therefore, the detected F should correspond to either F grafted on the surface of TiO_2 by substitution of the surface hydroxyl groups or physico-sorbed F.[19,24] The doping concentration of F estimated by XPS spectra is around 0.97 at%. The Ti 2p and O 1s in XPS spectra coming from Ti−O−Ti linkages in TiO_2 also showed significant changes upon Fluorine incorporation. Compared with the undoped HS (457.2 and 462.9 eV for Ti $2p_{3/2}$ and Ti $2p_{1/2}$), the binding energy of Ti $2p_{3/2}$ and Ti $2p_{1/2}$ increased to 459.4 and 465.2 eV after fluorine-doping (as shown in Figure 4), indicating the different electronic interactions of Ti with anions, which causes partial electron transfer from Ti to F and a decrease in the electron density of Ti because of the lower electron negativity of fluorine compared to oxygen. Also, a decrease in the full width at half-maximum of the Ti $2p_{3/2}$ peak from 1.52 to 1.18 eV is observed after F- HS TiO_2. This peak narrowing phenomenon is related to the reduction in defect density of the HS TiO_2 by F-doping, which will be a benefit for electron transporting in TiO_2.[29]

X-ray diffraction patterns of HS and F-HS TiO_2 are shown in Figure 3, which indicate that both HS and F-HS TiO_2 mainly contain anatase TiO_2 phase. The crystal size D of anatase phase of undoped and F-doped TiO_2 hollow sphere is estimated from the (101) peak according to the Scherrer equation, $D = 0.89\lambda/\beta\cos\theta$, where λ, β, and θ refer to X-ray wavelength (0.15418 nm), the half-maximum width, and the Bragg's angle, respectively. The calculated D is about 21.8 nm for HS and 19.9 nm for F-HS TiO_2, respectively. As shown in inset of Figure 3, the F-doping reduces the percentage of brookite phase in TiO_2 hollow sphere, from 18.1% to 9.2%. This is due

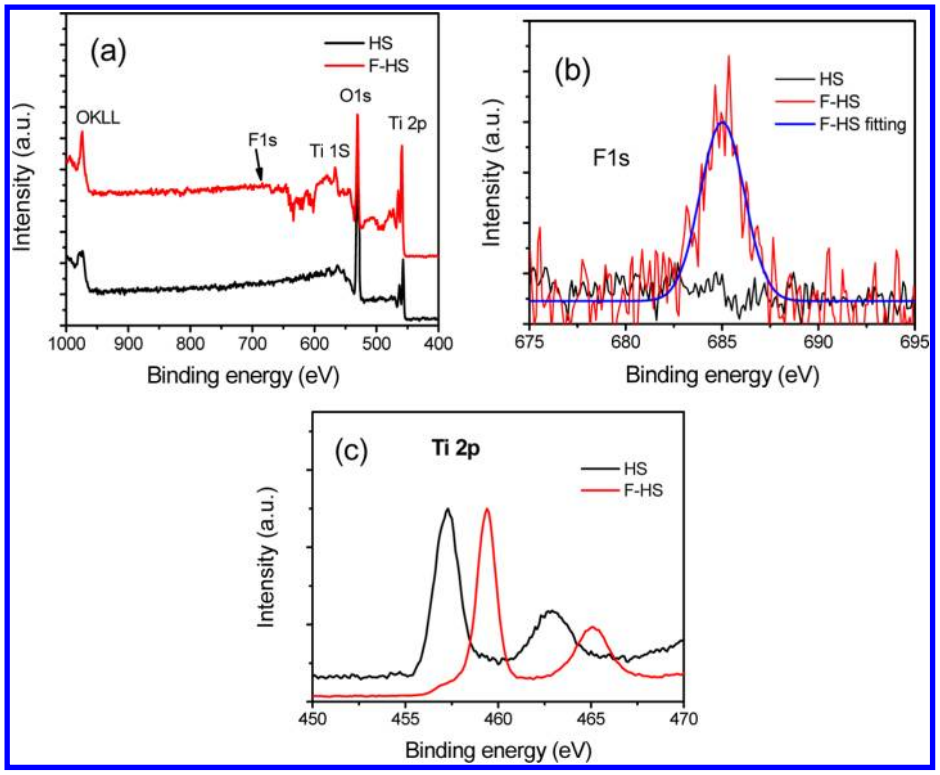

Figure 2. XPS spectra of the undoped and F-doped TiO_2 hollow spheres (a). F 1s region (b) and high-resolution XPS of the Ti 2p (c).

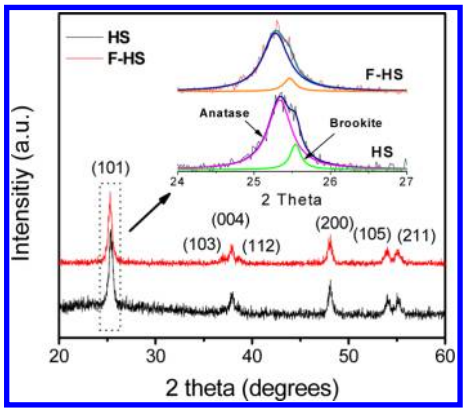

Figure 3. XRD patterns of HS and F-HS TiO_2 powder.

to the F^- ions suppressing the crystallization of brookite by adsorbing onto the surfaces of TiO_2 particles.[20] A high percentage of anatase phase would be a benefit for the DSSCs due to its higher charge transport ability.[30]

As discussed above, F-doping could reduce the defect density of TiO_2 hollow sphere and increase the percentage of anatase phase in TiO_2 hollow, which will be a benefit for charge transport in TiO_2 hollow structure. To investigate the F-doping of TiO_2 hollow sphere on the photovoltaic properties of the devices, the HS and F-HS TiO_2 scattering layers were formed on the transparent TiO_2 film (paste from Solaronix) to fabricate double layered photoelectrodes (devices **2** and **3**, respectively), the control photoelectrode without scattering layer (device **1**) also was fabricated for comparison. Figure 3a shows the incident photon-to-current efficiency (IPCE) curves of different photoelectrodes. The device **2** has higher IPCE values in the range of 350−550 nm than that of device **1**, which is attributed to enhancement of light harvesting by Mie scattering effect and multiple reflections in the interior of the hollow structures.[2,16−18] It is noted that IPCE spectrum of device **3** is

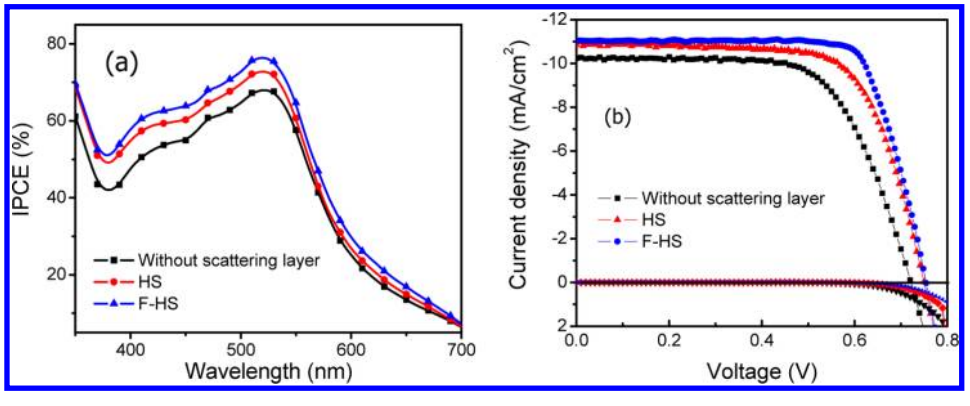

Figure 4. IPCE spectra of different photoelectrodes (a). *J*−*V* characteristics of different photoelectrodes under AM 1.5 G 100 mW/cm^2 (b).

dx.doi.org/10.1021/am300801f | ACS Appl. Mater. Interfaces 2012, 4, 3712−3717

Table 1. Performance Parameters of Photovoltaic Devices Based on Different TiO_2 Scattering Layer Photoelectrodes[a]

devices	J_{sc} (mAcm^{-2})	V_{oc} (V)	FF (%)	η (%)	adsorbed dye[b] (nmol·cm^{-2})	surface area (m^2 g^{-1})	porosity (%)
1	10.16	0.720	65.9	4.80	34.5	50[c]	
2	10.80	0.750	69.4	5.62	38.0	77.1	70.0
3	11.00	0.754	76.1	6.31	39.0	78.3	71.5

[a]The active area of the photoelectrodes is 0.16 cm^2. [b]The dye adsorbed on TiO_2 film was desorbed by a 0.1 M NaOH solution (water/ethanol 1:1 v/v) for 24 h. [c]BET data is obtained from Wuhan Geao Instruments Science and Technology Co. Ltd.

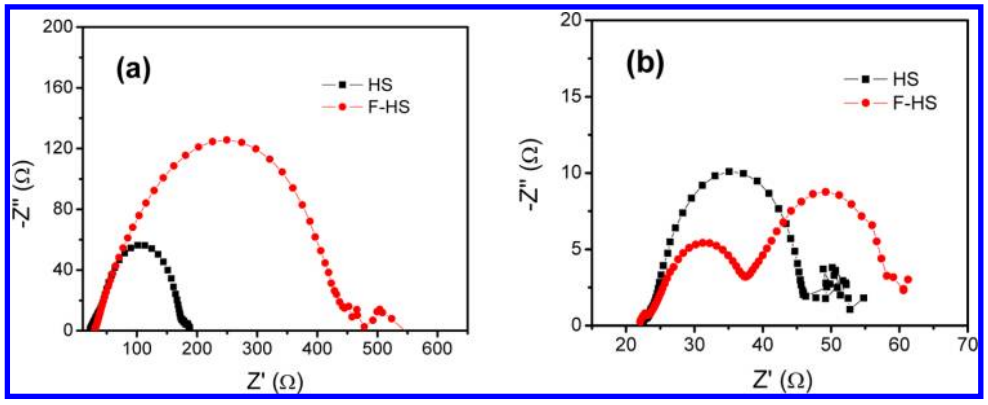

Figure 5. Nyquist plots of electrochemical impedance spectra of devices **2** and **3** in dark (a) and under illumination conditions (b).

quite similar to the device **2**, just slightly higher than that in the whole response range of the device (350−700 nm), which indicates F-doping has no significant impact on the scattering effect of the hollow sphere and the light harvesting of photoelectrode, although the F-doped hollow sphere has smaller crystalline sizes and better crystallinity (as shown in the XRD results) that is reported to affect the visible-light absorption and light-scattering.[31] It could be explained that UV-light is not able to reach the scattering layer through the 13 μm TiO_2 layer since the light penetration limit in TiO_2 is less than 1 μm.

The photovoltaic properties ($J-V$ curves) of the devices were studied under AM 1.5 illumination (100 mW/cm^2) (Figure 3b). The short-circuit current densities (J_{sc}), open-circuit voltages (V_{oc}), and fill factors (FF) of devices were summarized in Table 1. The overall conversion efficiency was obtained on the basis of the equation, $\eta = J_{sc} \times V_{oc} \times FF/P_{in} \times 100\%$ where P_{in} is the incident radioactive flux. In comparison with the device **1** (without scattering layer), the overall conversion efficiency (η) of device **2** (HS TiO_2 scattering layer) is increased by 17%, from 4.8% to 5.62%. The performance of photoelectrode is further enhanced by about 13% using F-HS TiO_2 hollow sphere as scattering layer resulting from the significantly enhanced fill factor (increased by ∼10%) of devices, compared with the photoelectrode based on non F-doped TiO_2 hollow sphere, which reaches 6.31% with a J_{sc} = 11.0 mA/cm^2, V_{oc} = 0.754 V, and FF = 76.1%. The $J-V$ characteristics in the dark were performed to obtain some evidence for the increased FF and J_{sc}. As shown in Figure 5, the dark current onset of F-HS TiO_2 device shifts to higher potential, in comparison with TiO_2−HS device, and the dark-current of device **3** is smaller than that of device **2** at the same potential, indicating larger parallel resistance (recombination resistance) in F-HS device. Furthermore, the slope of $J-V$ curve near open-circuit voltage of F-HS device shows a slight increment, which is corresponding to the reduction of series resistance of DSSCs. On the basis of the $J-V$ curve and generalized Shockley equation used to study solar cell, FF of DSSC is mainly decided by the recombination rate of electrons. Therefore, the significantly enhanced FF of devices can be attributed to the reduced charge recombination and enhanced charge transfer in a device with F-doped TiO_2 as scattering layer.[32] The beneficial effect of F doping on device performance can be explained by retarding the charge recombination through TiO_2 surface states by reducing oxygen vacancies via formation of the Ti−F bond and improving charge transport by a high percentage of anatase phase.

To further confirm the effects of F-doping on electron transport in the TiO_2 network and electron recombination between the injected electron and the redox electrolyte (I_3^-), we carried out electrical impedance spectroscopy (EIS) measurements as shown in Figure 5. In the dark at −0.69 V bias, no electrons were injected from dye sensitizer into TiO_2 network, electrons were just transported through the interconnected TiO_2 nanoparticles, after which they reacted with the redox electrolyte (I_3^-). Thus, the charge-transfer resistance at the TiO_2/dye/electrolyte interface (R_{ct}) in the dark and under forward bias is related to the recombination process between the electrons at conducting band of TiO_2 nanoparticle and the electrolyte. This is estimated from the middle semicircle (1−10^2 Hz) in the Nyquist plots of EIS measured in the dark.[33−40] Parameters obtained from EIS are summarized in Table 2. The R_{ct} values of devices **2** and **3** are estimated to be 150.0 and 410.7 Ω, respectively. The

Table 2. Recombination Resistance (R_{ct}), Electron Transport Resistance (R_t), Effective Electron Life Time (τ), and Electrolyte Diffusion Constant ($D_{I_3^-}$)

devices	R_{ct} (Ω cm^2)	R_t (Ω cm^2)	τ (ms)[a]	$D_{I_3^-}$ (×10^{-6}cm^2/s)
2	150	22.3	50.4	2.0
3	410.7	13.9	74.6	2.2

[a]Acquired by the inversion of frequency of the maximum imaginary impedance component at the medium frequency ($1/2\pi f_{max}$) of the semicircle.

recombination resistance is nearly two times increased using F-HS as scattering layer. This means that F-HS device is better in retarding recombination between electrons at conducting band of TiO_2 nanoparticle and the electrolyte. Furthermore, the electron transport resistance (R_t) was estimated from the Nyquist plots. Under the illumination and open circuit voltage condition, R_t is 22.3 and 13.9 Ω for devices **2** and **3**, respectively, indicating faster electron transport in device **3** in comparison to that of device **2**. Faster electron transport and low charge recombination rate in devices result in longer electron lifetime in devices in comparison to device **2** (50.4 and 74.6 ms for device **2** and **3**, respectively). Therefore, from the analysis of EIS, the same conclusion as that from $J-V$ curves can be obtained, the F-doping reduced the trap states in TiO_2 surface, thus decreasing the charge transfer resistance and significantly increasing the recombination resistance between photoelectrode and electrolyte, resulting in a dramatic increase of FF and utilization of photogenerated electron.

In addition, the F-doping caused noteworthy change in the low frequency region of impedance spectra of devices. The semicircle in the low frequency (10^{-2}–1 Hz) region is related to the electrolyte diffusion and the impedance of electrolyte diffusion described by Nernst equation as follows,[38,39] $Z_n = (W/(i\omega)^{1/2})$ tan h $(((i\omega)/(K_N))^{1/2})$, where W is the Warburg parameter $W = ((kT)/(n^2e_0^2c_{I_3^-}A(D_{I_3^-})^{1/2}))$ and $K_N\delta^2 = D_{I_3^-}$; $D_{I_3^-}$ is electrolyte diffusion constant, A is the electrode area, e_0 is the elementary charge, k is Boltzmann constant, n is the number of electrons transported in each reaction (in general, $n = 2$), T is the temperature, δ is the thickness of Nernst diffusion layer, which is half of the distance between the electrodes).[41−44] The diffusion constant is 2.0×10^{-6} and 2.2×10^{-6} cm^2/s for devices **2** and device **3**, respectively. The analysis of EIS indicates that the use of F-doped TiO_2 as an active scattering layer can significantly improve current collection due to faster electron and electrolyte transport, resulting in significant enhancement in FF and PCE of DSSCs.

4. CONCLUSION

In summary, we have investigated the photovoltaic properties of F-doping of TiO_2 hollow spheres in dye-sensitized solar cells. In comparison to the photoanode with the nondoped TiO_2 hollow spheres as the scattering layer, the overall conversion efficiency of the F-doped HS TiO_2 photoanode is increased by 13%. The use of F-doped TiO_2 hollow spheres as the active scattering layer can significantly improve current collection due to faster electron, higher electrolyte diffusion ability, and reduced electron loss from the grain boundary scattering and low recombination at the TiO_2/electrolyte interface. It is worthy of note that a better DSSC efficiency can be achieved by fabrication of the thickness of TiO_2 photoanode equal or close to the electron diffusion length. If the thickness of TiO_2 photoanode (bottom transparent TiO_2 film + scattering layer) in this work is not optimized, it is possible to further improve the device performance and is planned to be conducted. This work demonstrates a multifunctional scattering layer and provides a promising strategy to explore high-efficiency DSSCs.

AUTHOR INFORMATION

Corresponding Author

*E-mail: wongcc@ntu.edu.sg (C.C.W.); xuewei@ntu.edu.sg (X.-W.L.); ecmli@ntu.edu.sg (C.M.L.).

Author Contributions

#These authors contributed equally to this work.

Notes

The authors declare no competing financial interest.

ACKNOWLEDGMENTS

This work was supported by a Singapore National Research Foundation Grant under NRF-CRP2-2007-02, AcRF Tier 2 (ARC 24/07, No. T206B1218RS, and ARC 10/10, No. MOE2010-T2-1-060) from MOE, and CREATE program (Nanomaterials for Energy and Water Management) from NRF, funding (RG54/07 and SUG41/06).

REFERENCES

(1) Grätzel, M. *Nature* **2001**, *414*, 338.
(2) Ito, S.; Murakami, T. N.; Comte, P.; Liska, P.; Grätzel, C.; Nazeeruddin, M. K.; Grätzel, M. *Thin Solid Films* **2008**, *516*, 4613.
(3) Atwater, H. A.; Polman, A. *Nat. Mater.* **2010**, *9*, 205213.
(4) Chen, T.; Guai, G. H.; Gong, C.; Hu, W.; Zhu, J.; Yang, H.; Yan, Q.; Li, C. M. *Energy Environ. Sci.* **2012**, *5*, 6294.
(5) Guai, G. H.; Leiw, M. Y.; Ng, C. M.; Li, C. M. *Adv. Energy Mater.* **2012**, *2*, 334.
(6) Guo, C. X.; Yang, H. B.; Sheng, Z. M.; Lu, Z. S.; Song, Q. L.; Li, C. M. *Angew. Chem., Int. Ed.* **2010**, *49*, 3014.
(7) Guo, C. X.; Guai, G. H.; Li, C. M. *Adv. Energy Mater.* **2011**, *1*, 448.
(8) Yang, H. B.; Guai, G. H.; Guo, C. X.; Song, Q. L.; Jiang, S. P.; Wang, Y.; Zhang, W.; Li, C. M. *J. Phys. Chem. C* **2011**, *115*, 12209.
(9) Meng, H.; Yang, Y.; Chen, Y.; Zhou, Y.; Liu, Y.; Chen, X.; Ma, H.; Tang, Z.; Liu, D.; Jiang, L. *Chem. Commun.* **2009**, *17*, 2293.
(10) Gao, Y.; Tang, Z. *Small* **2011**, *7*, 2133.
(11) Dong, Z.; Lai, X.; Halpert, J. E.; Yang, N.; Yi, L.; Zhai, J.; Wang, D.; Tang, Z.; Jiang, L. *Adv. Mater.* **2012**, *24*, 1046.
(12) Du, J.; Qi, J.; Wang, D.; Tang, Z. *Energy Environ. Sci.* **2012**, *5*, 6914.
(13) Kang, S. H.; Choi, S.-H.; Kang, M.-S.; Kim, J.-Y.; Kim, H.-S.; Hyeon, T.; Sung, Y. E. *Adv. Mater.* **2008**, *20*, 5458.
(14) Koo, H. J.; Kim, Y. J.; Lee, Y. H.; Lee, W. I.; Kim, K.; Park, N. G. *Adv. Mater.* **2008**, *20*, 195.
(15) Park, N. G.; Kim, K. M.; Kang, M. G.; Ryu, K. S.; Chang, S. H.; Shin, Y. J. *Adv. Mater.* **2005**, *17*, 2349.
(16) Qian, J. F.; Liu, P.; Xiao, Y.; Jiang, Y.; Cao, Y. L.; Ai, X. P.; Yang, H. X. *Adv. Mater.* **2009**, *21*, 3663.
(17) Tian, Z. P.; Tian, H. M.; Wang, X. Y.; Yuan, S. K.; Zhang, J. Y.; Zhang, X. B.; Yu, T.; Zou, Z. G. *Appl. Phys. Lett.* **2009**, *94*, 031905.
(18) Frank, A. J.; Kopidakis, N.; van de Lagemaat, J. *Coord. Chem. Rev.* **2004**, *248*, 1169.
(19) Yang, H. B.; Guo, C. X.; Guai, G. H.; Song, Q.; Jiang, S. P.; Li, C. M. *ACS Appl. Mater. Interfaces* **2011**, *3*, 1940.
(20) Yu, J. C.; Yu, J.; Ho, W.; Jiang, Z.; Zhang, L. *Chem. Mater.* **2002**, *14*, 3808.
(21) Lu, X.; Mou, X.; Wu, J.; Zhang, D.; Zhang, L.; Huang, F.; Xu, F.; Huang, S. *Adv. Funct. Mater.* **2010**, *20*, 509.
(22) Kim, C.; Kim, K. S.; Kim, H. Y.; Han, Y. S. *J. Mater. Chem.* **2008**, *18*, 5809.
(23) Feng, X. J.; Shankar, K.; Paulose, M.; Grimes, C. A. *Angew. Chem., Int. Ed.* **2009**, *48*, 8095.
(24) Samadpour, M.; Boix, P. P.; Giménez, S.; Iraji Zad, A.; Taghavinia, N.; Mora-Seró, I.; Bisquert, J. *J. Phys. Chem. C* **2011**, *115*, 14400.
(25) Hore, S.; Nitz, P.; Vetter, C.; Prahl, C.; Niggemann, M.; Kern, R. *Chem. Commun.* **2005**, *15*, 2011.
(26) Wang, X.; Song, J. L.; Yip, C. H.; Wong, C. C.; Liu, X. W. *Nanosci. Nanotech. Lett.* **2011**, *3*, 191.
(27) Yu, J. C.; Yu, J. G.; Ho, W. K.; Jiang, Z. T.; Zhang, L. Z. *Chem. Mater.* **2002**, *14*, 3808.
(28) Liu, S. W.; Yu, J. G.; Mann, S. *Nanotechnology* **2009**, *20*, 325606.

(29) Oh, W. S.; Xu, C.; Kim, D. Y.; Goodman, D. W. *J. Vac. Sci. Technol., A* **1997**, *15*, 1710.
(30) Hsiao, P.-T.; Wang, K.-P.; Cheng, C.-W.; Teng, H. *J. Photochem. Photobiol., A* **2007**, *188*, 19.
(31) Dai, G.; Zhao, L.; Li, J.; Wan, L.; Hu, F.; Xu, Z.; Dong, B.; Lu, H.; Wang, S.; Yu, J. *J. Colloid Interface Sci.* **2012**, *365*, 46.
(32) Fabregat-Santiago, F.; Bisquert, J.; Palomares, E.; Otero, L.; Kuang, D. B.; Zakeeruddin, S. M.; Grätzel, M. *J. Phys. Chem. C* **2007**, *111*, 6550.
(33) Nakade, S.; Makimoto, Y.; Kubo, W.; Kitamura, T.; Wada, Y.; Yanagida, S. *J. Phys. Chem. B* **2005**, *109*, 3488.
(34) Oekermann, T.; Zhang, D.; Yoshida, T.; Minoura, H. *J. Phys. Chem. B* **2004**, *108*, 2227.
(35) Huang, S. Y.; Schlichthrl, G.; Nozik, A. J.; Grätzel, M.; Frank, A. J. *J. Phys. Chem. B* **1997**, *101*, 2576.
(36) Duffy, N. W.; Peter, L. M.; Rajapakse, R. M. G.; Wijayantha, K. G. U. *J. Phys. Chem. B* **2000**, *104*, 8916.
(37) Wang, Q.; Moser, J. E.; Grätzel, M. *J. Phys. Chem. B* **2005**, *109*, 14945.
(38) Adachi, M.; Sakamoto, M.; Jiu, J. T.; Ogata, Y.; Isoda, S. *J. Phys. Chem. B* **2006**, *110*, 13872.
(39) Kern, R.; Sastrawan, R.; Ferber, J.; Stangl, R.; Luther, J. *Electrochim. Acta* **2002**, *47*, 4213.
(40) Hauch, A.; Georg, A. *Electrochim. Acta* **2001**, *46*, 3457.
(41) Mor, G. K.; Shankar, K.; Paulose, M.; Varghese, O. K.; Grimes, C. A. *Nano Lett.* **2006**, *6*, 215.
(42) Bisquert, J.; Zaban, A.; Greenshtein, M.; Mora-Seró, I. *J. Am. Chem. Soc.* **2004**, *126*, 13559.
(43) Meekins, B. H.; Kamat, P. V. *ACS Nano* **2009**, *3*, 3437.
(44) Bang, J. H.; Kamat, P. V. *Adv. Funct. Mater.* **2010**, *20*, 1970.